

Nonequilibrium relaxation and scaling properties of the two-dimensional Coulomb glass in the aging regime

MATTHEW T. SHIMER, UWE C. TÄUBER, and MICHEL PLEIMLING

Department of Physics, Virginia Polytechnic Institute and State University, Blacksburg, VA 24061-0435

PACS 75.10.Nr – Spin-glass and other random models
 PACS 05.70.Ln – Theories and models of many-electron systems
 PACS 71.55.Jv – Disordered structures; amorphous and glassy solids

Abstract. - We employ Monte Carlo simulations to investigate the two-time density autocorrelation function for the two-dimensional Coulomb glass. We find that the nonequilibrium relaxation properties of this highly correlated disordered system can be described by a full aging scaling ansatz. The scaling exponents are non-universal, and depend on temperature and charge density.

Introduction. – Exploring the nature of relaxation from out-of-equilibrium initial states towards stationary thermal equilibrium has been a major focus of nonequilibrium statistical mechanics (for a comprehensive current overview, see, e.g., Ref. [1]). Fundamental questions concern the scaling properties of two-time correlation functions in the so-called aging regime (to be discussed more extensively below), namely: (1) What are the basic scaling forms to describe numerical and experimental data? (2) Are the ensuing scaling exponents and scaling functions universal? (3) Which physical properties determine the scaling features in the aging regime? Aside from contributing to our still rather incomplete understanding of processes far from equilibrium, providing comprehensive and reliable answers to questions (2) and (3) could have important ramifications to materials science as well. For example, a clear picture of which features of nonequilibrium relaxation processes contain specific information on the system under investigation in contrast to which properties are generic may provide a novel method of sample characterization. To this end, various model systems have been carefully investigated through numerical simulations; a few simple models even allow for analytical treatments [1].

Disordered semiconductors in the vicinity of a metal-insulator transition constitute an intriguing experimental system displaying complex relaxation phenomena. Relaxation measurements for the conductivity of a two-dimensional silicon sample have yielded unambiguous evidence for aging effects [2], see also Ref. [3]. The interpretation of these experiments continues to build upon the

early theoretical predictions of Coulomb glass models [4–6] that incorporate the essential physical aspects of charge carriers localized at random positions in space and interacting through long-range forces. Research into the non-trivial equilibrium properties [7–15] and non-equilibrium relaxation phenomena [16–24] of the Coulomb glass over the past two decades have considerably advanced our understanding of this paradigmatic model system for highly correlated disordered materials. Our goal in this paper is to examine the fundamental questions (1)–(3) for the Coulomb glass in two dimensions, with the aim to better understand universality aspects and scaling properties of disordered semiconductors. (We note that a very similar model, with the Coulomb potential essentially replaced by a logarithmic repulsion, describes the Bose glass phase of magnetic flux lines in type-II superconductors that are pinned to columnar defects, see Refs. [25–27].) Specifically, we address the detailed scaling form for the two-time density autocorrelation function, and the dependence on temperature and carrier density of the non-equilibrium relaxation kinetics. Our work builds upon and extends the investigations of Gempel *et al.* who employed a very similar Monte Carlo simulation method [20, 21]; however, we decided to extend our studies to multiple carrier densities in addition to varying temperatures. This allows us to study in a very systematic way the aging properties of the two-dimensional Coulomb glass, utilizing different scaling forms for the density autocorrelation function (see also Ref. [28] in the context of a spin glass model).

The Coulomb glass model and Monte Carlo simulation procedure. – Our basic model system is a

Coulomb glass in two dimensions. The Coulomb glass model, introduced by Efros and Shklovskii [4], consists of multiple localized pinning sites available to the charge carriers. Because of the strong intra-site correlations these sites can only contain a single charge carrier at most. The system is dominated by long-range repulsive Coulomb interactions $V(r) \sim 1/r$ and the spatial disorder is induced by the randomly located (on a continuum) available sites. The Hamiltonian of the Coulomb glass model reads [4–6]

$$H = \sum_i n_i \varphi_i + \frac{e^2}{2\kappa} \sum_{i \neq j} \frac{(n_i - K)(n_j - K)}{|\mathbf{R}_i - \mathbf{R}_j|}, \quad (1)$$

where \mathbf{R}_i , φ_i , and n_i respectively denote the position vector (here in two dimensions), (bare) site energy, and occupancy of the i th site, $i = 1, \dots, N$. The occupancy n_i can only take on the values 0 or 1. The first term corresponds to (random) site energies assigned to each accessible location; since the system is dominated by the long-range forces, we chose $\varphi_i = 0$ to further simplify the model, while still allowing the positions \mathbf{R}_i to be continuous and random [9, 17, 20]. (Alternatively, one could allow φ_i to take on random values while the positions \mathbf{R}_i would be discrete and set on a lattice.) The second contribution encapsulates the repulsive Coulomb interactions (with dielectric constant κ). In order to maintain global charge neutrality, a uniform relative charge density $K = \sum_i n_i / N$ is inserted; K can also be described as the total carrier density per site, or filling fraction. We note that with $\varphi_i = 0$ the Hamiltonian (1) displays particle–hole symmetry, i.e., systems with $K = 0.5 + k$ and $K = 0.5 - k$ are equivalent. Upon replacing the occupation numbers with spin variables $\sigma_i = 2n_i - 1 = \pm 1$, one sees that the Coulomb glass maps onto a random-site random-field antiferromagnetic Ising model with long-range exchange interactions [7].

We employ a Monte Carlo simulation algorithm to at least heuristically model the kinetics in the Coulomb glass [20, 21]. At each time step, one randomly selected charge carrier attempts to hop from an occupied site a to an empty site b . Two factors determine the hopping success rate, namely a strongly distance-dependent tunneling process (in semiconductors mediated through phonons) and thermally activated jumps over energy barriers [20], i.e.,

$$\Gamma_{a \rightarrow b} = \tau_0^{-1} e^{-2R_{ab}/\xi} \min[1, e^{-\Delta E_{ab}/T}], \quad (2)$$

where τ_0 represents a microscopic time scale, $R_{ab} = |\mathbf{R}_a - \mathbf{R}_b|$ is the distance between sites a and b , ξ characterizes the spatial extension of the localized carrier wave functions, and we have set $k_B = 1$. The first, spatially exponential term in (2) is derived from quantum tunneling, while the second exponential term is due to thermodynamics: A thermally activated hop from sites a to b entails the energy difference

$$\Delta E_{ab} = \epsilon_b - \epsilon_a - \frac{e^2}{\kappa R_{ab}}, \quad (3)$$

with the (interacting) site energies

$$\epsilon_a = \frac{e^2}{\kappa} \sum_{b \neq a} \frac{n_b - K}{R_{ab}}. \quad (4)$$

In the following, distances are measured relative to the average separation between sites a_0 , and energies as well as temperature scales are measured relative to the typical Coulomb energy $E_C = e^2/\kappa a_0$ [20]. We set the spatial extension of the localized wave functions, ξ , to a_0 , as in Refs. [20, 21]. We have explored other values for ξ as well, and (within the applicability range of the model) found the ensuing results to simply scale with τ_0 ; hence $\xi = a_0$ was chosen for simplification.

The Monte Carlo simulations were initiated by randomly placing N sites within a square simulation cell of length L containing $N_e = KN$ charge carriers, where $N = L^2$. We performed simulations for systems with $L = 8, 10, 16, 32$; with temperatures in the range of $0.01 \leq T \leq 0.05$; and carrier densities in the range of $0.375 \leq K \leq 0.5$ (also equivalent to $0.5 \leq K \leq 0.625$ due to particle–hole symmetry). Running the simulations with various system sizes L , we noticed no measurable finite-size effects, as demonstrated in Fig. 2(a). Temperatures larger than 0.03 turned out not to be useful for our study of aging processes since equilibrium was then reached far too quickly. In contrast, for $T < 0.01$, the kinetics slowed down too much for gathering statistically significant data within computationally reasonable time frames. As will be discussed in more detail below, the dynamics also freezes out within the numerically accessible simulation times for $K < 0.4$ (or $K > 0.6$).

Periodic boundary conditions were used and the potential due to charges outside the cell was calculated by mirroring the simulation cell on each side. Initially, the charge carriers were placed randomly at available sites to mimic a quench from very high temperatures. Then the system was evolved at temperature T with the dynamics described by the generalized Metropolis rate (2). The thermally activated, tunneling-controlled (variable-range) hopping algorithm begins with randomly choosing an occupied site a and assigning a normalized probability proportional to $\exp(-2R_{ab}/\xi)$ to each empty site. An empty site b is then chosen from this probability distribution and a hop from a to b is attempted. The success probability for this move is determined by $\min[1, e^{-\Delta E_{ab}/T}]$. There are N hop attempts for each Monte Carlo step (MCS). Our simulation runs consisted of 1×10^6 MCS and results were averaged over 3000 different realizations of the initial conditions and of the random number sequences.

In thermal equilibrium, the long-range correlations and spatial disorder conspire to produce a soft gap in the (interacting) density of states $g(\epsilon)$, as famously first noted by Efros and Shklovskii [4]. The repulsive interactions induce strong spatial anticorrelations, which in turn suppress the availability of states with energies close to the chemical potential μ_c that at $T = 0$ separates the occupied and

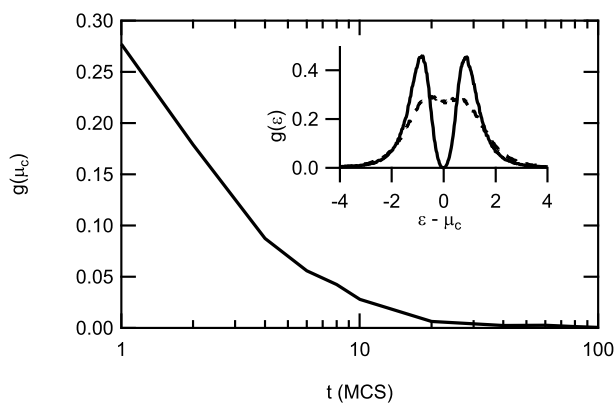


Fig. 1: Coulomb gap formation in a Coulomb glass ($L = 16$, $N = 256$ sites) at half filling $K = 0.5$ and at temperature $T = 0.02$. The plot shows how $g(\mu_c)$ quickly approaches zero. The density of states is displayed in the inset at $t = 1$ MCS (dashed) and $t = 100$ MCS (solid), when the Coulomb gap correlations are clearly established.

empty energy levels. The ensuing Coulomb gap appears to asymptotically be described by a power law $g(\epsilon) \sim |\epsilon - \mu_c|^s$ [5–14]; within a simple mean-field approach, $s = (d/\sigma) - 1$ in d dimensions for a system with long-range repulsive potential $V(r) \sim 1/r^\sigma$. We have monitored the emergence of the Coulomb gap in our Monte Carlo simulations. Quite remarkably, the soft gap forms very fast, as illustrated in Fig. 1, which shows how the density of states at the chemical potential $g(\mu_c)$ quickly approaches zero. Indeed, the Coulomb gap is already pronounced after as few as 10 MCS, and clearly established in less than 100 MCS. In the following, we proceed to carefully analyze the slow decay of local density correlations; we remark that the interesting aging kinetics happens in a time period when the Coulomb gap itself is already well-established and therefore addresses slow dynamics in a highly correlated disordered system.

Scaling properties or the two-time density autocorrelation function in the aging regime. – In the following, we focus on the (normalized) two-time carrier density autocorrelation function [20],

$$C(t, s) = \frac{\langle n_i(t)n_i(s) \rangle - K^2}{K(1-K)} = \frac{\sum_i n_i(t)n_i(s) - NK^2}{NK(1-K)}, \quad (5)$$

where $t > s$, and the waiting time s refers to the time elapsed since the high-temperature quench (initiation of the Monte Carlo simulations). If both s and t are large compared to microscopic time scales τ_0 , and also well separated, i.e., if

$$t \gg \tau_0, \quad s \gg \tau_0, \quad t - s \gg \tau_0, \quad (6)$$

time-translational invariance is broken and C depends on both t and s separately. In the aging scaling regime, one then expects the autocorrelation function to obey the gen-

eral scaling form (we follow the notation in Ref. [1]),

$$C(t, s) = s^{-b} f_C(t/s^\mu). \quad (7)$$

For certain simple systems obeying purely relaxational dynamics, namely the one-dimensional kinetic Ising model [29, 30], the time-dependent Ginzburg–Landau models quenched to a critical point, [31, 32] and the spherical model A coarsening dynamics in the low-temperature phase, with short-range [33, 34] or long-range [35–37] interactions, the aging scaling regime is amenable to analytic treatment. In these cases one finds that the ansatz (7) is satisfied with exponent $\mu = 1$, a situation commonly referred to as full aging scaling. For more complex systems such as spin glasses the possibility of a subaging scaling with $\mu < 1$ [1] has been discussed in the literature. For $\mu = 1$ and $t/s \rightarrow \infty$ the full aging scaling function follows a power law [1],

$$f_C(t/s) \sim (t/s)^{-\lambda_C/z}, \quad (8)$$

with the autocorrelation exponent λ_C and the dynamic exponent z . Overall, this presents us with three scaling exponents: b , μ , and λ_C/z .

From the averaged charge density autocorrelation function (5) we extracted the scaling exponents using an interpolation method motivated by Ref. [38]. The total variance, or spread, of the data was calculated by comparing the data points to polynomial interpolations of all other curves. This variance was only measured within the scaling regime. We have chosen to either assume full aging scaling, $\mu = 1$ in Eq. (7), and applied the polynomial interpolation method to obtain the scaling exponent $b > 0$; or to set $b = 0$ (simple scaling ansatz) and alternatively determine the subaging exponent $\mu < 1$.

Sample sets of results (with $L = 16$, $N = 256$ sites) are shown in Figs. 2 and 3. The density autocorrelation data at half filling $K = 0.5$ displayed in Fig. 2(a) match nicely with the results of Ref. [20]; however, the scaling forms used in Figs. 2(b) and 2(c) are different from those employed by Grempel. As is apparent from Fig. 2(a), the density autocorrelation function is characterized by two temporal regimes. In the first time regime, the density autocorrelation relaxes towards a plateau (often referred to as β relaxation in the glass literature), whereas in the second time regime the system very slowly approaches equilibrium (α relaxation) [39, 40]. This later regime displays breaking of time translation invariance and aging scaling, provided the inequalities (6) hold. With our current algorithm and available hardware, we cannot effectively investigate systems with densities lower than $K = 0.40625$ and temperatures lower than $T = 0.02$, since in these configurations the plateau regions persist for much longer times than are computationally accessible for us, i.e., the system essentially freezes into a structure that corresponds to the β relaxation plateau. Notice that the autocorrelation data obtained for a smaller system ($L = 10$, $N = 100$ sites) coincide with those for the larger system, demonstrating the absence of finite-size effects in the observed time window.

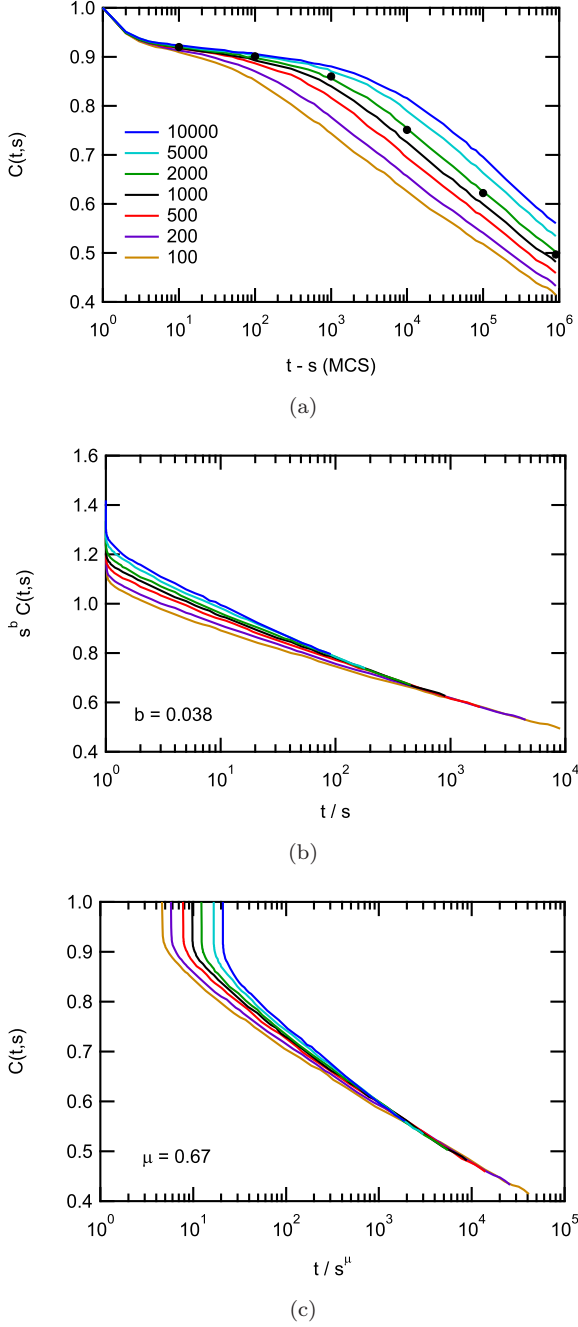


Fig. 2: Carrier density autocorrelation function $C(t,s)$ at half filling $K=0.5$, in a system of linear extension $L=16$ ($N=256$ sites) at temperature $T=0.02$, measured for various waiting times $s=10^2, 2 \times 10^2, 5 \times 10^2, 10^3, 2 \times 10^3, 5 \times 10^3, 10^4$ (from bottom to top). (a) The plot vs. $t-s$ demonstrates the breaking of time-translation invariance. The \bullet symbols represent data obtained from a system of length $L=10$ ($N=100$ sites). (b) A full aging scaling plot, which assumes $\mu=1$, yields the scaling exponents $b=0.038$ and $\lambda_C/z=0.103$. (c) A subaging scaling analysis, fixing $b=0$, gives $\mu=0.67$.

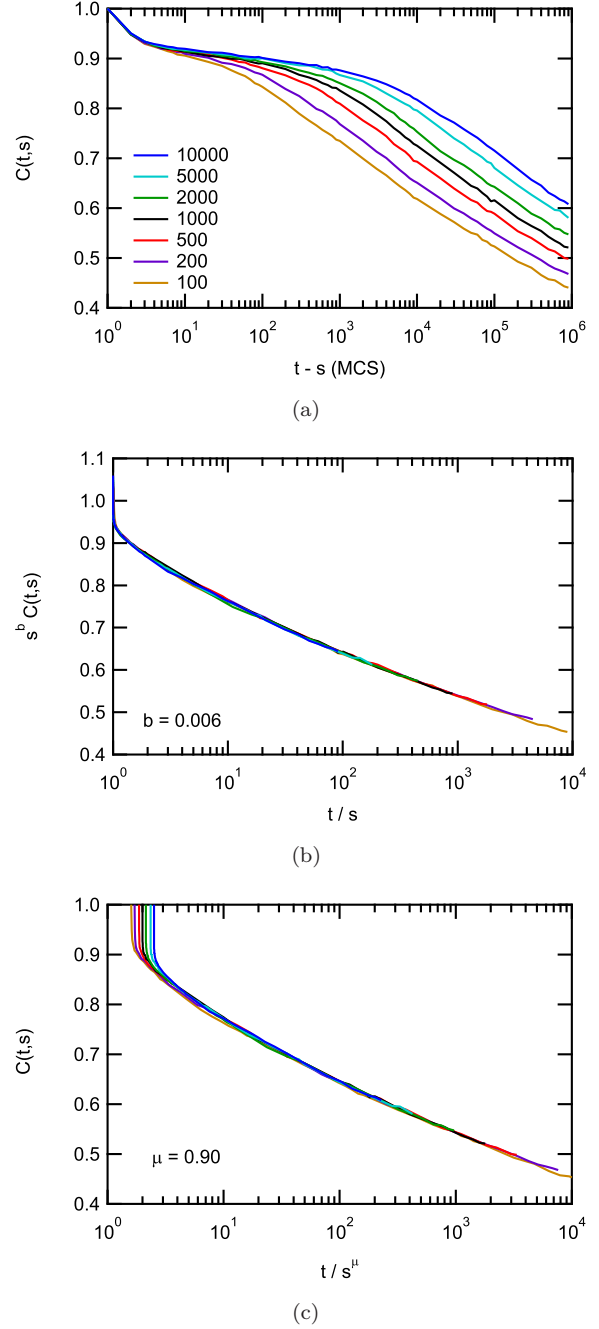


Fig. 3: (a) Carrier density autocorrelation function $C(t,s)$ at carrier density $K=0.4375$ (again with $L=16$, $N=256$, and $T=0.02$), measured for various waiting times $s=10^2, 2 \times 10^2, 5 \times 10^2, 10^3, 2 \times 10^3, 5 \times 10^3, 10^4$ (from bottom to top). Note the markedly slower decay as compared to the data at half filling shown in Fig. 2. (b) A full aging scaling plot ($\mu=1$) gives $b=0.006$ and $\lambda_C/z=0.075$. (c) A subaging scaling analysis ($b=0$) results in $\mu=0.90$.

Table 1: Charge carrier density dependence of the full aging scaling exponents b and λ_C/z (with $\mu = 1$ and $T = 0.02$).

K	b	λ_C/z
0.40625	0.001 ± 0.002	0.046 ± 0.004
0.4375	0.006 ± 0.002	0.075 ± 0.004
0.46875	0.021 ± 0.004	0.089 ± 0.003
0.5	0.038 ± 0.006	0.103 ± 0.004

Table 2: Temperature dependence of the full aging scaling exponents b and λ_C/z (with $\mu = 1$ and $K = 0.5$).

T	b	λ_C/z
0.01	-0.001 ± 0.001	0.036 ± 0.004
0.02	0.038 ± 0.006	0.103 ± 0.004
0.03	0.080 ± 0.008	0.173 ± 0.005

Table 3: Charge carrier density dependence of the subaging exponent μ (with $b = 0$ and $T = 0.02$).

K	μ
0.40625	1.00 ± 0.01
0.4375	0.90 ± 0.01
0.46875	0.78 ± 0.01
0.5	0.67 ± 0.02

Table 4: Temperature dependence of the subaging exponent μ (with $b = 0$ and $K = 0.5$).

T	μ
0.01	0.98 ± 0.06
0.02	0.67 ± 0.02
0.03	0.54 ± 0.02

In Fig. 2(b), we plot the same data as in Fig. 2(a), after applying a rescaling procedure that assumes full aging (where $\mu = 1$). One notes that the systematic deviations for small t become less and less important for increasing waiting times s . From the scaling ansatz (7), which is well founded theoretically [1], the scaling exponent b can be reliably extracted from the data sets corresponding to larger waiting times. As expected from Eq. (8), a power law is observed at long times, which in turn yields the scaling exponent λ_C/z . At half filling $K = 0.5$, we find $b = 0.038 \pm 0.006$ and $\lambda_C/z = 0.103 \pm 0.004$. Alternatively, we may employ a subaging scaling ansatz, setting $b = 0$. Figure 2(c) shows the results from scaling using μ only. Also in this case deviations are observed for t small, but an improvement is less apparent when increasing the waiting time. Collapsing the data on a single master curve at large scaling arguments works apparently about equally well with either method employed in (b) or (c). In fact, allowing nontrivial values for both scaling exponents, $b > 0$ and $\mu < 1$, yields comparable scaling collapse quality. However, given that theoretical analysis (admittedly for comparatively simple systems) yields the full aging scenario with $\mu = 1$ and generally $b > 0$, we would argue that subaging scaling, as used in previous studies [20,21], need not be invoked to describe the nonequilibrium relaxation phenomena in the Coulomb glass.

Figure 3 shows the results when the same scaling methods are applied to our data for relative charge carrier density $K = 0.4375$ (or $K = 0.5625$). As the carrier density deviates from half filling, the relaxation becomes markedly slower. The full aging scaling ansatz ($\mu = 1$) yields an excellent data collapse for all s and t values. The same conclusion holds for other charge carrier densities $K \neq 0.5$. For $K = 0.4375$, from the scaling analysis based on Fig. 3(b) we infer the rather low value $b = 0.006 \pm 0.002$ along with $\lambda_C/z = 0.075 \pm 0.004$. If we instead assume $b = 0$, the subaging scaling from Fig. 3(c) gives $\mu = 0.90 \pm 0.01$. Clearly, the aging scaling expo-

nents are *not* universal in the Coulomb glass, but strongly depend on the charge carrier density. At least near half-filling, in the time window that is accessible to us we observe power-law scaling, albeit with numerically small exponent values b and λ_C/z , different from, but close to the logarithmic dependence obtained by the mean-field type analysis in Refs. [22,23].

We ran sets of 3000 simulation runs each at various values of T and K to systematically explore the dependence of the aging scaling exponents on the temperature (already noted in Refs. [20,21]) and carrier density. The resulting exponent values for b and λ_C/z as obtained within the full aging framework (setting $\mu = 1$) are listed in Tables 1 and 2. Physically, smaller values of the exponents imply slower relaxation kinetics. The trend that is observed is that as density drops away from half filling, the relaxation slows. A similar trend is seen in the temperature dependence; namely, the relaxation processes become slower at lower temperatures, as one would naturally expect. If, on the other hand, we enforce $b = 0$ and instead allow for the subaging scaling scenario, we find the exponent values μ listed in Tables 3 and 4. Note that a larger value of μ leads to slower relaxation. The dependence of the subaging exponent thus follows the same qualitative trends as observed in full aging scaling. Naturally, as in the full aging scaling analysis the exponent b approaches zero at low temperatures or away from half-filling, in the subaging scaling analysis $\mu \rightarrow 1$. (In fact, for either $T = 0.01$ or $K = 0.40625$ our simulations approach the aforementioned limitations in run times; we list the corresponding exponent values with large relative errors nevertheless, since they still confirm the general trends.) We remark that our findings for the scaling of nonequilibrium relaxation processes in the Coulomb glass align well with a recent study of the aging kinetics in the two-dimensional ferromagnetic Ising model with uniform bond disorder: Ref. [41] also finds non-universal scaling exponents, depending on the ratio of disorder distribution width and temperature.

Conclusion. – We have investigated nonequilibrium relaxation processes of the two-dimensional Coulomb glass model at low temperatures via Monte Carlo simulations, and confirmed that its scaling features are governed by the simple aging scaling form. Through the use of polynomial interpolation methods, three scaling exponents were extracted and found to follow a common trend: as either the temperature decreases or the charge carrier density deviates more from half-filling, the exponents reflect slower relaxation kinetics. The aging scaling exponents are thus found to be non-universal, as is the case for disordered magnetic systems [41]. Our results indicate that the inclusion of a subaging exponent $\mu \neq 1$ is unnecessary since a nonzero scaling exponent b encapsulates the same characteristics, and the corresponding simple aging scaling form is more firmly grounded on theoretical analysis.

We are presently working on extending the scope of our study into three dimensions. Preliminary data for the density autocorrelation function scaling in the aging regime suggest the same basic features and trends that we observe in two dimensions [42]. We also plan to implement logarithmic repulsion instead of the $1/r$ potential used in the Coulomb glass, with the aim to study aging phenomena in the Bose glass phase of type-II superconductors with columnar defects [25–27]. Our ultimate goal will be to more closely relate our observables and findings to experimental setups and measurements.

This work was supported by the U.S. Department of Energy, Office of Basic Energy Sciences (DOE–BES) under grant no. DE-FG02-09ER46613. We gladly acknowledge stimulating discussions with Ariel Amir, Malte Henkel, and Dragana Popović.

REFERENCES

- [1] HENKEL M. and PLEIMLING M., *Nonequilibrium Phase Transitions, Volume 2: Ageing and Dynamical Scaling Far From Equilibrium* (Springer, New York) 2010.
- [2] JAROSZYŃSKI J. and POPOVIĆ D., *Phys. Rev. Lett.*, **99** (2007) 046405 & 216401.
- [3] GRENET T. and DELAHAYE J., *Eur. Phys. J. B*, **76** (2010) 229.
- [4] EFROS A. L. and SHKLOVSKII B. I., *J. Phys. C*, **8** (1975) L49.
- [5] SHKLOVSKII B. I. and EFROS A. L., *Electronic Properties of Doped Semiconductors* (Springer, New York) 1984.
- [6] EFROS A. L. and POLLAK M. (Editors), *Electron–Electron Interactions in Disordered Systems* (North-Holland, Amsterdam) 1985.
- [7] DAVIES J. H., LEE P. A., and RICE T. M., *Phys. Rev. Lett.*, **49** (1982) 758.
- [8] GRÜNEWALD M., POHLMANN B., SCHWEITZER L., and WÜRTZ D., *J. Phys. C*, **15** (1982) L1153.
- [9] XUE W. and LEE P. A., *Phys. Rev. B*, **38** (1988) 9093.
- [10] MÖBIUS A., RICHTER M., and DRITTLER B., *Phys. Rev. B*, **45** (1992) 11568.
- [11] GRANNAN E. R. and YU C. C., *Phys. Rev. Lett.*, **71** (1993) 3335.
- [12] MENASHE D., BIHAM O., LAIKHTMAN, B. D., and EFROS A. L., *Europhys. Lett.*, **52** (2000) 94.
- [13] MENASHE D., BIHAM O., and LAIKHTMAN, B. D., *Phys. Rev. B*, **64** (2001) 115209.
- [14] SURER B., KATZGRABER H. G., ZIMANYI G. T., ALLGOOD B. A., and BLATTER G., *Phys. Rev. Lett.*, **102** (2009) 067205.
- [15] GOETHE M. and PALASSINI M., *Phys. Rev. Lett.*, **103** (2009) 045702.
- [16] PÉREZ-GARRIDO A., ORTUÑO M., and CUEVAS E., *Phys. Rev. B*, **59** (1999) 5328.
- [17] YU C. C., *Phys. Rev. Lett.*, **82** (1999) 4074.
- [18] DÍAZ-SÁNCHEZ A. AND PÉREZ-GARRIDO A., *Eur. Phys. J. B*, **24** (2001) 483.
- [19] TSGANKOV D. N., PAZY E., LAIKHTMAN B. D., and EFROS A. L., *Phys. Rev. B*, **68** (2003) 184205.
- [20] GREMPEL D. R., *Europhys. Lett.*, **66** (2004) 854.
- [21] KOLTON A. B., GREMPEL D. R., and DOMÍNGUEZ D., *Phys. Rev. B*, **71** (2005) 024206.
- [22] AMIR A., OREG Y., AND IMRY Y., *Phys. Rev. B*, **77** (2008) 165207.
- [23] AMIR A., OREG Y., AND IMRY Y., *Phys. Rev. Lett.*, **103** (2009) 126403.
- [24] KIRGENGEN M. and BERGLI J., *Phys. Rev. B*, **79** (2009) 075205.
- [25] NELSON D. R. and VINOKUR V. M., *Phys. Rev. B*, **48** (1993) 13060.
- [26] TÄUBER U. C., DAI H., NELSON D. R., and LIEBER C. M., *Phys. Rev. Lett.*, **74** (1995) 5132.
- [27] TÄUBER U. C. and NELSON D. R., *Phys. Rev. B*, **52** (1995) 16106.
- [28] BERTHIER L. and BOUCHAUD J.-P., *Phys. Rev. B*, **66** (2002) 054404.
- [29] GODRÈCHE C. and LUCK J. M., *J. Phys. A: Math. Gen.*, **33** (1151) 2000.
- [30] LIPPIELLO E. and ZANNETTI M., *Phys. Rev. E*, **61** (3369) 2000.
- [31] JANSSEN H. K., SCHAUB B. and SCHMITTMANN B., *Z. Phys. B*, **73** (1989) 539.
- [32] CALABRESE P. and GAMBASSI A., *J. Phys. A: Math. Theor.*, **38** (2005) R133.
- [33] CONIGLIO A. and ZANETTI M., *Phys. Rev. B*, **42** (1990) 6873.
- [34] BIROLI G., *J. Stat. Mech.*, (2005) P05014.
- [35] CANNAS S. A., STARIOLO D. A. and TAMARIT F. A., *Physica A*, **294** (362) 2001.
- [36] BAUMANN F., DUTTA S. B. and HENKEL M., *J. Phys. A: Math. Gen.*, **40** (7839) 2007.
- [37] DUTTA S. B., *J. Phys. A: Math. Gen.*, **41** (395002) 2008.
- [38] BHATTACHARJEE S. M. and SENO F., *J. Phys. A: Math. Gen.*, **34** (2001) 6375.
- [39] GÖTZE W. and SJOGREN L., *Rep. Prog. Phys.*, **55** (1992) 241.
- [40] DEBENEDETTI P. G. and STILLINGER F. H., *Nature*, **410** (2001) 259.
- [41] HENKEL M. and PLEIMLING M., *Phys. Rev. B*, **78** (2008) 224419.
- [42] SHIMER M. T., TÄUBER U. C., and PLEIMLING M., *work in progress*, (2010) .